Advances in Nano Research, *Vol. 19, No. 5 (2025) 465-480*
https://doi.org/10.12989/anr.2025.19.5.465

Assessing mechanical and microstructural performance of ultra-high performance geopolymer mortar with micro activators under thermal curing

Ahmed Babeker Elhag[1,2], Nejib Ghazouani*[3] and Zeeshan Ahmad**[4]

[1]*Department of Civil Engineering, College of Engineering, King Khalid University, PO Box 394, Abha 61411 Saudi Arabia*
[2]*Center for Engineering and Technology Innovations, King Khalid University, Abha 61421, Saudi Arabia*
[3]*Mining Research Center, Northern Border university, Arar, 73213, Saudi Arabia*
[4]*Department of Civil Engineering, QCET, 57000, Pakistan*

(*Received March 5, 2025, Revised October 19, 2025, Accepted October 27, 2025*)

Abstract. This research develops and evaluates ultra-high performance geopolymer mortar (UHPGM) incorporating micro-activators and municipal solid waste incineration fly ash (MFA) as a sustainable supplementary cementitious material under thermal curing (60°C for 48 h). The study aims to enhance mechanical performance, durability, and eco-efficiency by optimizing binder composition and curing conditions. Five mix designs containing varying proportions of silica fume (SF), metakaolin (MK), and MFA were tested for workability, density, compressive strength, drying shrinkage, capillary water absorption, and elastic modulus. Microstructural and mineralogical analyses were conducted using SEM/EDS, XRD, and TGA/DTG to elucidate hydration and gel formation mechanisms. Results revealed that MFA improved workability by 36.1% owing to its low water absorption and fine particle morphology. All UHPGM mixes achieved compressive strengths above 100 MPa, with the SF-rich mix reaching 134.5 MPa. Ternary blends containing MFA and MK demonstrated a favorable balance of strength, density, and dimensional stability. SF significantly reduced drying shrinkage (by ~24%) and capillary absorption, forming dense C-(A)-S-H and (C,N)-A-S-H gels that enhanced microstructural compactness. Thermal curing promoted calcite formation and secondary hydration, reducing porosity and strengthening interfacial bonding. The findings highlight MFA's potential as a low-cost, eco-friendly alternative in producing sustainable UHPGC, capable of delivering high mechanical performance and durability while supporting waste valorization and carbon reduction goals in modern construction materials.
Keywords: capillary water absorption; municipal solid waste incineration fly ash (MFA); scanning electron microscopy (SEM); shrinkage; sustainability; ultra-high performance geopolymer composite (UHPGC)

1. Introduction

Portland cement and other inorganic binders each have unique advantages and disadvantages when it comes to material performance, economic effectiveness, and environmental impact. Finding substitute binder systems and additional cementitious materials has become more important as a result of the significant CO_2 emissions connected to the production of Portland cement. Alkali-activated materials (AAMs) have become a very promising substitute among these. Because of the creation of distinct reaction products, these materials not only drastically reduce CO_2 emissions but also show improved durability when compared to binders based on Portland cement. The aluminosilicate sources utilized in AAMs demonstrate strong reactivity in alkaline media, primarily because of their fine particle size and amorphous or nanocrystalline nature, comparable to that of cement. Common precursors for AAMs include fly ash, metakaolin (MK), and ground granulated blast furnace slag (Kamble *et al*. 2014, Khater 2016, Farazin and Mohammadimehr 2020, Sokhandani *et al*. 2022).

Ultra-high-performance geopolymer composites (UHPGCs) have been successfully engineered by combining cutting-edge techniques like the incorporation of mineral admixtures, a reduced water-to-binder ratio, thermal curing, the use of superplasticizers, and matrix packing density optimization. UHPGCs with exceptional mechanical strength and durability are the result of these advancements (Salahaddin *et al*. 2022, Abellan-Garcia *et al*. 2023, Fan *et al*. 2023, Moula *et al*. 2023, Zhang *et al*. 2023). However, compared to normal concrete, the cost of making UHPGC might be up to nine times greater per cubic meter (Dong 2018). Consequently, the utilization of low-cost and sustainable raw materials, particularly those derived from processed solid waste, has become an attractive solution for reducing production costs and environmental impacts (Al-Naghi *et al*. 2024, Elhadi *et al*. 2024, Ghazouani *et al*. 2024).

The hydration events that result in the creation of calcium silicate hydrate (C-S-H) gels are primarily responsible for the remarkable mechanical performance of hardened UHPGC, particularly its compressive strength. The material's overall performance is improved by these reactions, which also increase the material's microstructural density. Heat curing and the high rate of supplementary

*Corresponding author, Ph.D.,
E-mail: nejib.ghazouani@nbu.edu.sa
**Co-corresponding author, Professor,
E-mail: zeeshanlaskani@gmail.com

ISSN: 2287-237X (Print), 2287-2388 (Online)

cementitious material (SCM) incorporation have a significant impact on the formation of such hydrated phases (Richard and Cheyrezy 1995, Khater and Abd El Gawwad 2015, Huang *et al*. 2022). Silica fume (SF), quartz powder, MK, fly ash, rice husk ash, furnace slag, and recycled glass are common SCMs utilized in UHPGC systems (Pyo *et al*. 2018, Adnan *et al*. 2024, Ahmed *et al*. 2024, Al-Naghi *et al*. 2025a, b, Alashker *et al*. 2025). Despite these achievements, further research is required to elucidate the exact influence of mineral admixtures on the hydration mechanisms and the resulting properties of UHPGC, particularly under early-age thermal curing conditions.

Thermal treatment significantly decreased the dioxin concentration in MFA, reducing it to just 1/1209 of its initial value and thereby minimizing potential health and environmental risks (Lv *et al*. 2022). When this treated MFA was used to replace 20% of cement in ultra-high-performance concrete (UHPC), it enhanced hydration kinetics, decreased workability, shortened setting time, and improved the 28-day compressive strength. The modified matrix exhibited fine, harmless pores (<20 nm) and demonstrated strong immobilization of heavy metal ions, underscoring MFA's suitability as an eco-efficient cement alternative in UHPC (Lv *et al*. 2022). The effectiveness of SCMs largely depends on the availability of key oxides such as Ca, Si, Al, and Fe, elements abundantly present in MFA. Given its compositional and functional similarity to conventional SCMs like pozzolans and fly ash, MFA shows promise for use in both cement-based and geopolymer binders (Zhan *et al*. 2024, Raza *et al*. 2025a, b, c, Elhag *et al*. 2025, Akbar *et al*. 2025, Kahla *et al*. 2025, Ghazouani *et al*. 2025). Furthermore, integrating MFA into geopolymer matrices has been found to stabilize its heavy metal content due to the robust three-dimensional aluminosilicate network, which can effectively adsorb and bind metal cations (Chu *et al*. 2024). These reaction products immobilize contaminants through both encapsulation and chemical complexation, ensuring stabilization of more than 98% of heavy metals present in MFA (Huang *et al*. 2024, Aydogdu 2014). This suggests that geopolymer produced with MFA is suitable for use in load-bearing concrete structures that are not exposed to leaching conditions, such as porous bricks, provided it is not subjected to acidic or neutral environments with prolonged moisture exposure. Because municipal fly ash (MFA) derived from waste incineration plants typically contains a high level of moisture, large macro-aggregates tend to develop, making pretreatment processes such as drying and milling necessary. Studies have shown that mechanical pretreatment not only improves the quality of MFA but also minimizes the leaching of heavy metals in the resulting products (Zhou and Li 2024).

The performance of geopolymer composites can be improved by optimization techniques and various SCMs, according to a number of studies (Mabrouk *et al*. 2024, Raza *et al*. 2024a, b, c). For instance, Zhang *et al*. (2019) used granite powder in place of 15% cement and SF to cure at 90 °C for 48 hours, resulting in a compressive strength of 182 MPa. Similarly, Wu *et al*. (2017) used steam and hot-water curing at 90 °C to achieve similar strengths by substituting granulated blast furnace slag and SF for 20% of cement. Under similar curing conditions, Guo *et al*. (2024) reported a strength of 135 MPa when fly ash was used as a partial cement substitute. In another study, Van *et al*. (2014) reached 185 MPa with hot-water curing at 65 °C and 90 °C by replacing 25% of cement with granulated slag and incorporating rice husk ash.

Despite extensive research on ultra-high performance geopolymer composites (UHPGCs), few studies have examined the combined effects of multiple micro-activators, such as SF, MK, and MFA, under controlled thermal curing conditions. The novelty of this study lies in integrating MFA, a sustainable waste-derived supplementary cementitious material, with conventional activators in a thermally cured UHPGC system to achieve ultra-high strength and durability at a reduced curing temperature and duration (60 °C for 48 h). This approach enhances the energy efficiency of the curing process while valorizing a hazardous byproduct into a functional binder component. By systematically evaluating the synergistic effects of SF, MK, and MFA on workability, strength development, durability indices, and microstructural evolution, the research offers new insights into optimizing binder composition and curing protocols for sustainable high-performance geopolymer systems. The results aid in the creation of UHPGC formulations that are low in carbon, economical, and ecologically friendly and that can be used in prefabricated structural applications. With compressive strengths exceeding 130 MPa under low-temperature curing, the developed ultra-high performance geopolymer mortar (UHPGM) showed great promise for real-world application in prefabricated structural elements, façade panels, bridge deck overlays, and repair materials where durability and quick strength gain are crucial. MFA refines the microstructure and lowers permeability, guaranteeing exceptional durability and facilitating its practical adoption in high-performance, low-carbon infrastructure applications. It also increases sustainability by recycling industrial by-products and reducing CO_2 emissions when compared to Portland cement systems.

2. Experimental setup

2.1 Materials

Portland cement that was procured locally, non-densified SF, metakaolin (MK), and modified fly ash (MFA) were used as SCMs in this investigation. Two washing cycles with tap water were used as part of the pretreatment phase before the MFA was used. To dissolve soluble components, MFA was combined with water in a 1:10 ratio (fly ash to water) for each cycle and thoroughly agitated. Following a 12-hour settling period, the mixture's supernatant—which contained dissolved salts and other contaminants—was extracted. To guarantee efficient purification, this washing procedure was repeated. The cleaned MFA was subsequently oven-dried at 105 °C to remove any remaining moisture before being incorporated into the geopolymer binder. The primary oxides present in

Table 1 Chemical composition and physical properties of binders

Compositions (wt%)	Cement	MFA	SF	MK
SiO_2	15.80	19.65	93.56	55.43
CaO	67.54	25.43	0.80	1.20
Al_2O_3	3.69	9.86	2.51	36.40
MgO	3.54	3.65	0.43	1.10
$CaCl_2$	-	12.32	-	-
K_2O	2.10	2.54	1.87	0.90
Fe_2O_3	1.98	5.48	0.23	3.87
SO_3	4.65	17.04	0.60	0.20
Na_2O	–	2.34	–	–
TiO_2	0.70	1.69	–	0.60
Density (g/cm^3)	3.17	2.64	2.20	2.63
BET (m^2/g)	2.80	12.65	17.45	16.73
Mean particle size (μm)	7.58	16.51	0.75	5.81

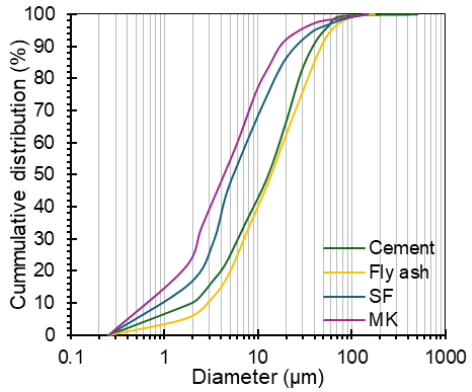

(a)

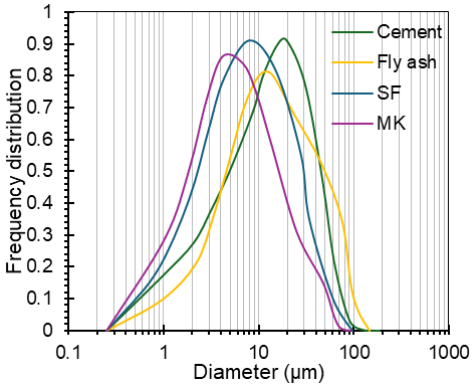

(b)

Fig. 1 Particle size distribution curves of cement and SCMs (a) cumulative distribution, and (b) frequency distribution

MFA were 25.43% CaO, 2.34% Na_2O, 19.65% SiO_2, 17.04% SO_3, and 12.32% $CaCl_2$, with particle sizes ranging between 1 and 20 μm.

The Portland cement exhibited a chemical composition of 3.69% Al_2O_3, 15.8% SiO_2, 4.65% SO_3, and 67.54% CaO. Its physical parameters included a specific gravity (SG) of 3.17 g/cm³, a surface area (SA) of 2.80 m²/g, and an average particle size (APS) of 7.58 μm. The silica fume had an SG of 2.20 g/cm³, SA of 17.45 m²/g, and an APS of 0.75 μm, with a composition of 93.56% SiO_2 and 2.51% Al_2O_3. Metakaolin possessed an SG of 2.63 g/cm³, SA of 16.73 m²/g, and APS of 5.81 μm, consisting mainly of 55.43% SiO_2 and 36.40% Al_2O_3. The detailed chemical and physical characteristics of the cement and SCMs are presented in Table 1.

The fine aggregate was sieved through an ASTM #30 mesh (600 μm) after being oven-dried for 24 hours at 110 °C. It had a fineness modulus of 1.45, a median particle size (d50) of 310 μm, and an SG of 2.66 g/cm³. The superplasticizer used in all mix formulations was Sika® ViscoCrete®-20 HE, which was dosed at 60 kg/m³. The admixture's SG ranged from 1.021 to 1.132 g/cm³, and its pH value ranged from 4 to 5. The cement and SCMs' particle size distribution curves are shown in Fig. 1.

2.2 Preparation of Specimens

In this research, five distinct mix formulations were designed, maintaining a constant water-to-binder (w/b) ratio of 0.17. Each mixture contained 825 kg/m³ of cement and 925 kg/m³ of sand. The binder compositions were proportioned such that SCMs made up 30% of the total binder mass, while Portland cement constituted the remaining 70%. Binary blends were formulated by combining Portland cement with either MFA (PC70SF0MK0MFA30), SF (PC70SF30MK0MFA0), or MK (PC70SF0MK30MFA0). For ternary systems, Portland cement was blended with both SF and MFA (PC70SF20MK0MFA10) or with SF and MK (PC70SF20MK10MFA0). In the ternary formulations, SF was partially substituted by 10% of each SCM by mass. The detailed mix proportions and constituent quantities for all formulations are presented in Table 2.

Regarding the issue of mineral deficiency, SF contributes reactive SiO_2, which promotes the consumption of portlandite generated during Portland cement hydration. This process results in the formation of an additional calcium silicate hydrate (C-S-H) gel, significantly enhancing the compressive strength and durability of ultra-high-performance geopolymer concrete (UHPGC). MK, due to its elevated SiO_2 and Al_2O_3 contents, not only supplies extra silica but also stimulates pozzolanic reactions, leading to matrix densification through the production of aluminum-rich hydrated phases. The presence of calcium–aluminum–silicate–hydrate (C-A-S-H) further reinforces the cementitious network and contributes to structural stability. To ensure homogeneity and prevent agglomeration of particles, the cement, SCMs, and fine aggregates were premixed prior to water addition (Soliman and Tagnit-Hamou 2017). The superplasticizer and mixing water were blended separately to form a uniform liquid phase. A mechanical mixer facilitated the mixing operation (Hiremath and Yaragal 2017, He *et al*. 2018). Initially, approximately 40% of the dry constituents and 50% of the liquid mixture were combined and mixed at a high speed for five minutes. To minimize material segregation and ensure adequate particle dispersion, the remaining components were gradually introduced in four successive stages, each lasting three minutes, at a lower mixing speed. Once all ingredients were incorporated, an additional five minutes of

Table 2 Mix design (kg/m³)

Mix ID	Sand	Cement	SF	MK	MFA	Superplasticizer	Water
PC70SF30MK0MFA0	925	825	280.5	–	–	60	187.9
PC70SF20MK10MFA0	925	825	181.5	99	–	60	187.9
PC70SF0MK30MFA0	925	825	–	280.5	–	60	187.9
PC70SF20MK0MFA10	925	825	181.5	–	99	60	187.9
PC70SF0MK0MFA30	925	825	–	–	280.5	60	187.9

high-speed mixing was applied to achieve a consistent and homogenous mix.

For microstructural analyses, including X-ray diffraction (XRD), thermogravimetric analysis (TGA), and scanning electron microscopy with energy-dispersive spectroscopy (SEM/EDS), prismatic specimens with 5 mm thickness were prepared. In accordance with ASTM C192M-19, freshly cast samples were immediately sealed with plastic film to prevent water evaporation and stored under standard curing conditions (25 °C and >95% relative humidity) for 24 hours (ASTM 2007). Following this initial curing, the molds were submerged in water for four hours prior to thermal treatment. Heat curing was conducted in an electric oven rated at 3000 W, with a controlled heating rate of 0.15 °C/min, maintaining an isothermal condition of 60 °C for 48 hours. After thermal curing, the specimens were cooled to ambient temperature and subsequently immersed in a saturated calcium hydroxide solution until the completion of mechanical and microstructural evaluations.

2.3 Testing of Specimens

The spread diameter in accordance with ASTM C230M-23 was In compliance with ASTM (2023), workability was evaluated. The mini-slump cone was raised right away to let the freshly prepared ultra-high-performance geopolymer concrete (UHPGC) spread. Two perpendicular diameters were measured once the spread stabilized, and the flow value was calculated by averaging them. Three different experiments were used to calculate the mean spread diameter. ASTM C138M-24 (ASTM 2024) was followed for density testing, in which the UHPGC mix was put into a cylindrical mold with a known volume that had been previously calibrated. The sample weight was determined once the surface was leveled, and density, which is the mass to volume ratio, was calculated. To ensure accuracy, this process was carried out three times.

Compressive strength (CS) testing adhered to ASTM C39M-18 (C39/C39M-18 2018). Six cylindrical specimens, each 50 mm in diameter and 100 mm in height, were tested under a controlled load rate of 0.250 MPa/s at curing ages of 7, 28, and 90 days. The mean compressive strength value was determined from the six readings.

Capillary water absorption (CWA) was measured using prismatic samples of 40 mm by 40 mm by 160 mm in accordance with ASTM C1585 (2013). The controlling formula is described in Ref. (Wu *et al*. 2024), and it was shown that there was a linear relationship between CWA and the square root of time (Wu *et al*. 2024). The samples were oven-dried at 60°C until they reached a consistent mass following a 28-day curing period. To guarantee precise measurement, epoxy glue was applied to the lateral surfaces and allowed to cure at room temperature. Following curing, the initial weights were noted, and testing for water absorption started as soon as the sample was submerged. Weight readings were taken at intervals from 1 to 400 minutes, wiping excess water within 30 seconds after removal. The average result from three specimens represented the CWA value.

Drying shrinkage (DS) was measured to evaluate the influence of SCMs and heat curing on UHPGC deformation. Measurements were taken between 3 and 120 days using a mortar shrinkage-expansion apparatus, and the linear shrinkage rate was computed based on the procedure reported by Li *et al*. (2023).

X-ray diffraction (XRD) on a JEOL JDX-3532 diffractometer with Cu Kα radiation and a tungsten filament running under vacuum was used to mineralogically characterize the 28-day UHPGC samples. Using a Mettler Toledo TGA/DSC 1 Stare system, thermal analysis of hydration products was carried out at 7, 14, and 28 days of curing. Specimens were vacuum-coated with a 400 Å thick coating of gold using a 10 mA current for two minutes in order to assess their microstructural integrity. Using a field-emission scanning electron microscope (SEM, ZEISS) running at 20 kV under high vacuum, surface morphology and phase distribution were investigated. Using energy-dispersive X-ray spectroscopy (EDS) in conjunction with the SEM, the elemental composition was examined.

3. Discussion of results

3.1 Flow and fresh density

Fig. 2 illustrates the workability and density results of the UHPGC mixtures. When individual SCMs were incorporated, the observed spread diameters were 285 mm for PC70SF30MK0MFA0, 252 mm for PC70SF0MK30MFA0, and 343 mm for PC70SF0MK0MFA30. The inclusion of MFA notably enhanced workability by 20.35% and 36.11% relative to the mixes containing SF and MK. The ultrafine SF particles, due to their higher specific surface area, increase the water demand in the binder system (Soliman and Tagnit-Hamou 2017). Although MK possesses a slightly lower specific surface area than SF, its irregular particle shape reduced the workability of PC70SF0MK30MFA0. Compared with PC70SF30MK0MFA0, this resulted in a

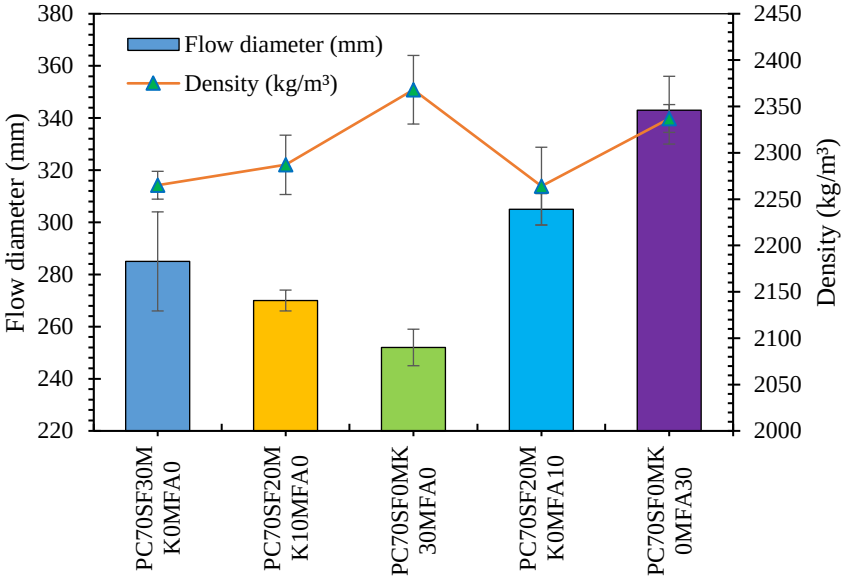

Fig. 2 Spread diameter and density results of mixes

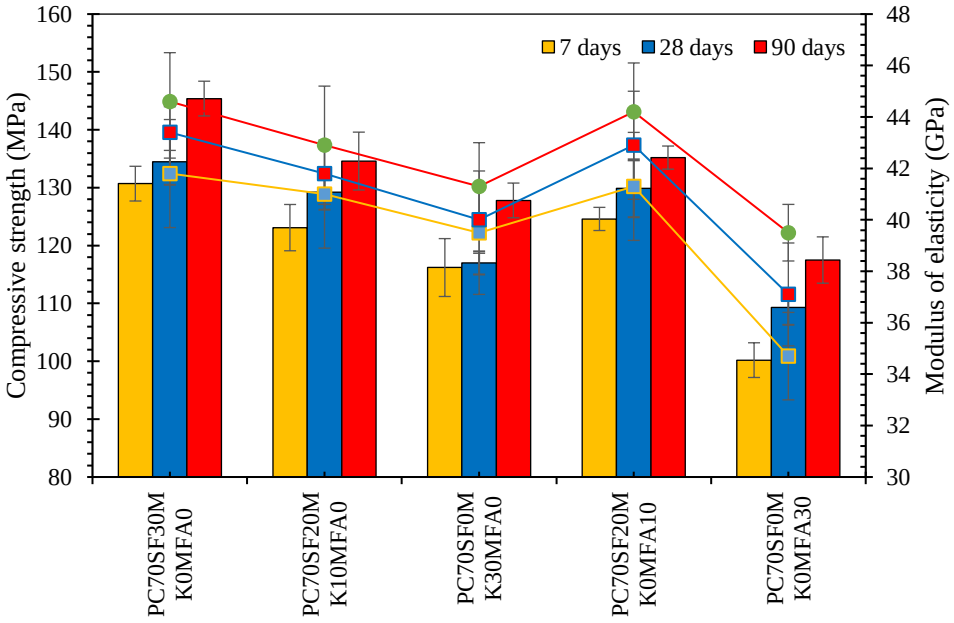

Fig. 3 CS and modulus of elasticity of mixes

13% lower spread diameter. This phenomenon can be attributed to the higher water requirement for wetting denser, irregularly shaped grains in the binder system, consistent with previous findings (Mo *et al*. 2020, Abdellatief *et al*. 2023).

A similar effect was evident when 10% of SF was replaced by MK (PC70SF20MK10MFA0), producing a spread diameter of 270 mm, which is 5.55% smaller than PC70SF30MK0MFA0. Conversely, substituting 20% of SF with MFA (PC70SF20MK0MFA10) increased the spread diameter to 305 mm, reflecting a 7.01% improvement in workability compared to PC70SF30MK0MFA0This enhancement is attributed to MFA's low intra-particle absorption, which promotes particle lubrication and improves fluidity, thereby reducing the requirement for water and superplasticizers (Soliman and Tagnit-Hamou 2017, Chu *et al*. 2022).

Regarding density, PC70SF0MK30MFA0 exhibited the highest value at 2368 kg/m³, followed by PC70SF0MK0MFA30 at 2337 kg/m³, and PC70SF30MK0MFA0 at 2265 kg/m³, corresponding to decreases of 1.32% and 4.54%, respectively. The inherent density of the SCMs influenced the resulting mixture densities when added to the binary combinations at equal 30% mass fractions. Ternary mixtures, PC70SF20MK10MFA0 and PC70SF20MK0MFA10, yielded densities of 2287 kg/m³ and 2264 kg/m³, respectively.

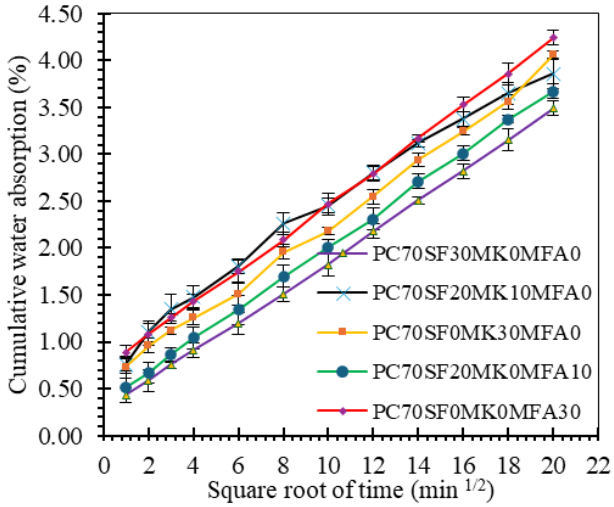

(a)

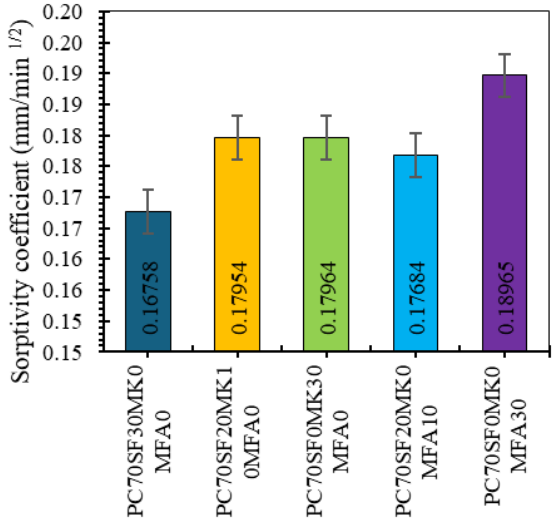

(b)

Fig. 4 Water absorption of UHPGC mixes (a) function of the square root of time and (b) sorptivity coefficient

3.2 Compressive strength and elastic modulus

Fig. 3 presents the compressive strength (CS) and modulus of elasticity results for the UHPGC systems at 7, 28, and 90 days. All mixtures achieved CS values above 100 MPa at each curing age (Dixit, Du *et al*. 2020), indicating that up to 150 kg/m³ of any of the SCMs can be effectively incorporated to produce ultra-high performance precast structural elements subjected to thermal treatment at 60°C. After 7 days, the PC70SF30MK0MFA0 mixture reached an average strength of 130.7 MPa, whereas PC70SF0MK30MFA0 and PC70SF0MK0MFA30 attained 116.2 MPa and 100.2 MPa, corresponding to decreases of 12.47% and 30.43%, respectively. At 28 days, PC70SF30MK0MFA0 achieved 134.5 MPa, with PC70SF0MK30MFA0 and PC70SF0MK0MFA30 showing 117 MPa and 109.3 MPa, indicating strength reductions of 14.95% and 23%. The enhanced performance of SF-containing mixtures can be attributed to the higher reactivity, finer particle size, and superior morphological uniformity of SF compared to MK, which facilitated better particle packing and improved the microstructure of the cementitious matrix. In contrast, MK and MFA produced lower strengths due to morphological and chemical limitations that restricted further strength development. After 90 days, PC70SF30MK0MFA0 achieved 145.4 MPa, while PC70SF0MK30MFA0 and PC70SF0MK0MFA30 reached 127.8 MPa and 117.5 MPa, representing reductions of 13.77% and 23.74%, respectively.

Ternary mixtures, such as PC70SF20MK10MFA0, exhibited strengths comparable to PC70SF30MK0MFA0, with slight decreases of 6.17% and 4.1% at 7 and 28 days. Similarly, PC70SF20MK0MFA10 achieved 124.6 MPa at 7 days, demonstrating that replacing 10% SF with MK or MFA produces comparable results. At 28 days, PC70SF20MK10MFA0 and PC70SF20MK0MFA10 reached 129.2 MPa and 129.9 MPa, respectively, showing only minor differences from PC70SF30MK0MFA0. This performance is attributed to the synergistic effect of the mineral admixtures in generating complementary hydrated phases that enhance strength at later ages. The comparable performance of PC70SF20MK0MFA10 highlights the feasibility of incorporating MFA, a solid waste-derived filler, into UHPGC mixtures, achieving strength levels similar to conventional SCMs like MK at reduced costs. These results align with previous studies on thermally cured UHPGC matrices containing MFA as an additional binder (Chu *et al*. 2022, Lu *et al*. 2022, Tran *et al*. 2023).

The calculated theoretical modulus of elasticity showed a strong correlation with compressive strength, consistent with prior UHPGC research (Al-Tikrite and Hadi 2017, Ahmad *et al*. 2019). This indicates a well-distributed granular skeleton and a discontinuous porosity network, both of which influence the material's elastic behavior. The highest elastic modulus was observed in PC70SF30MK0MFA0, reaching 41.8 GPa and 43.4 GPa at 7 and 28 days, respectively. The lowest modulus corresponded to the mixture with 30% MFA replacement, showing reductions of 20.46%, 16.98%, and 12.91% at 7, 28, and 90 days compared with the 30% SF-containing mixture.

3.3 Capillary water absorption

Water transport in UHPGC is predominantly driven by capillary suction resulting from surface tension (Zhu *et al*. 2023). In porous composites, both capillary absorption and water movement are characterized by the water absorption rate (Karataş *et al*. 2017). Figure 4 illustrates how different types of SCMs and curing regimes influence the capillary water absorption (CWA) rate of UHPGC. The data reveal a strong linear correlation (correlation coefficients > 0.97) between cumulative water uptake and the square root of time. The slope of this regression line represents the CWA rate (k), which serves as an indicator of the material's resistance to water penetration.

As shown in Fig. 4(b), reducing the SF proportion in the binder lowers the sorptivity coefficient (k) of UHPGC. For instance, the PC70SF30MK0MFA0 mixture exhibits a k

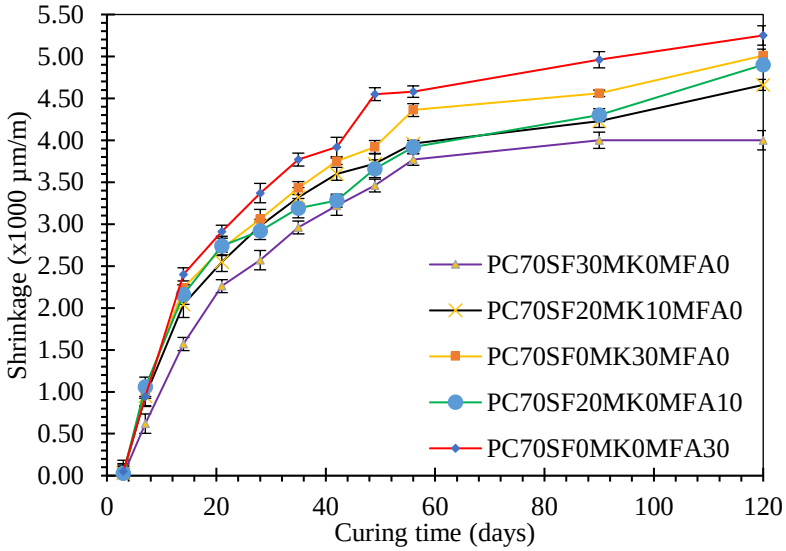

Fig. 5 Drying shrinkage characteristics of UHPGC mixes at different curing ages

value of 0.16758 mm/min$^{1/2}$, which is 13.16% lower than that of the PC70SF0MK0MFA30 mix. When the MK content reaches 30%, k rises to 0.17964 mm/min$^{1/2}$ but remains lower than the PC70SF0MK0MFA30 specimen containing 30% micro-filler alumina (MFA). This indicates that an optimal SF dosage effectively reduces UHPGC permeability. The observed reduction in k is attributed to the formation of calcium-alumino-silicate-hydrate and calcium/sodium-alumino-silicate-hydrate gels generated by SF incorporation, which block pore channels (Zhu *et al*. 2023). Additionally, the micro-filling effect of ultrafine SF refines the matrix structure, thereby modifying internal porosity.

The significant role of heated curing in enhancing UHPGC impermeability is evident. The decline in water absorption is likely associated with mechanisms that also improve compressive strength. Elevated-temperature curing encourages calcite formation, which either fills the pores (Beltrame *et al*. 2023) or reacts with calcium silicate hydrate gels to form new phases (Zhang *et al*. 2023). This results in a denser microstructure and a strengthened interfacial transition zone, thereby reducing porosity. Compared to standard curing, heated curing is not only more economical and environmentally favorable but also markedly enhances the mortar's resistance to water penetration.

3.4 Drying shrinkage

UHPGC specimens undergo drying shrinkage (DS) due to a combination of autogenous shrinkage, gel development, and the loss of water from capillary pores (Qu *et al*. 2020). This phenomenon significantly influences both the mechanical performance and long-term durability of UHPGC. Excessive shrinkage may cause cracking, which undermines structural integrity and overall performance. As illustrated in Fig. 5, the DS progression in UHPGC mixes containing various SCMs is rapid during the initial stages and gradually slows over time. By day 14, DS reaches approximately 30–70% of the total shrinkage measured at 28 days, indicating that most shrinkage occurs during the early strength-gaining period, after which the rate stabilizes. Increasing the SF proportion in the binder notably reduces the DS rate. The highest shrinkage, 5250 µm/m, is recorded for the PC70SF0MK0MFA30 mix, whereas the lowest, 4000 µm/m, is observed in the PC70SF30MK0MFA0 mix, which contains 30% SF replacement. This reduction is primarily due to the inclusion of SF (Zhang *et al*. 2023), which promotes polymerization, accelerates chemical reactions, decreases moisture loss, and fosters the formation of calcium-alumino-silicate-hydrate (C-A-S-H) and sodium-alumino-silicate-hydrate (N-A-S-H) gels. These gels fill the pores, stabilizing the internal structure and mitigating the elevated shrinkage typically seen in FA-based UHPGC.

Incorporating Portland cement and SF proves effective in reducing the drying shrinkage of UHPGC, leading to improved bond strength, lower porosity, and reduced permeability. Additionally, heated curing has a notable effect on drying shrinkage. It reduces moisture loss (Bakharev *et al*. 1999) and provides elevated temperatures (Castel *et al*. 2016), promoting efficient hydration reactions and thereby minimizing shrinkage. Though, extremely high temperatures during heated curing can have adverse effects, increasing the drying shrinkage rate of UHPGC.

3.6 Scanning electron microscopy with energy dispersive spectroscopy (SEM/EDS)

Fig. 6 presents the SEM/EDS analysis of the investigated mixes. The PC70SF30MK0MFA0 mixture exhibited remarkable density and a well-developed hydrated matrix, which corresponded to its high compressive strength of 134.5 MPa. Surface roughness and overlapping plate-like crystals observed in the SEM images correspond to the hydrated phases of calcium silicate hydrate (Tafraoui *et al*. 2016). The combination of high Ca, Si, and Al contents facilitated

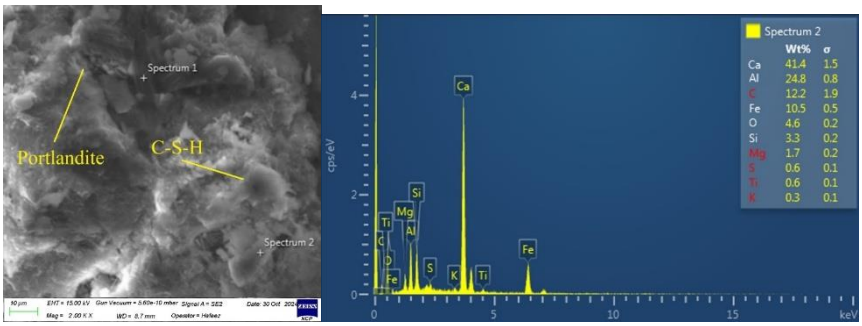

(a)

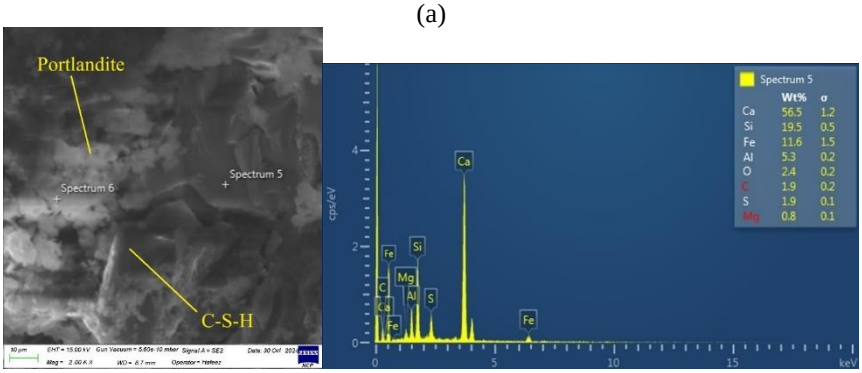

(b)

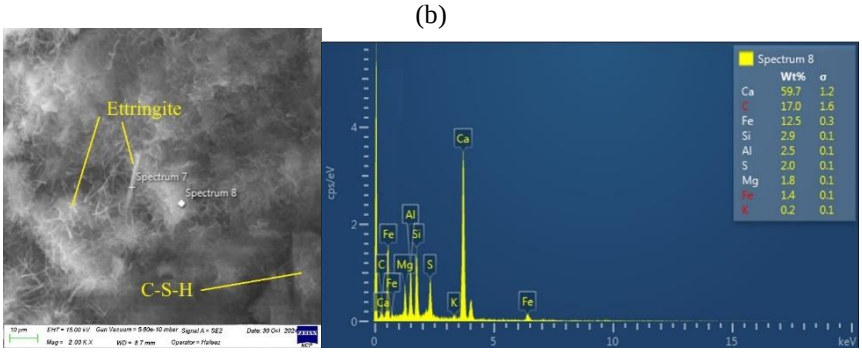

(c)

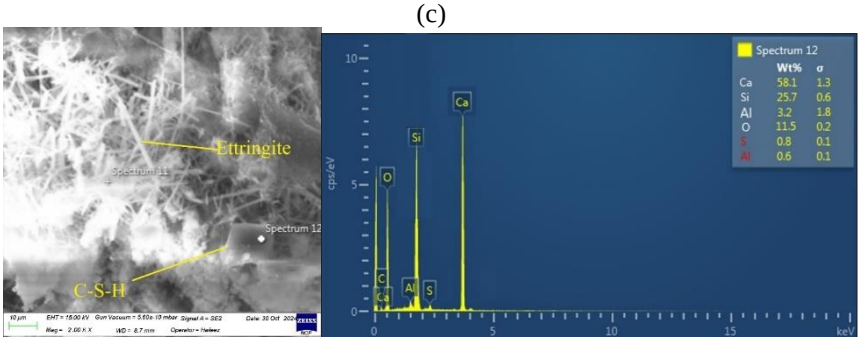

(d)

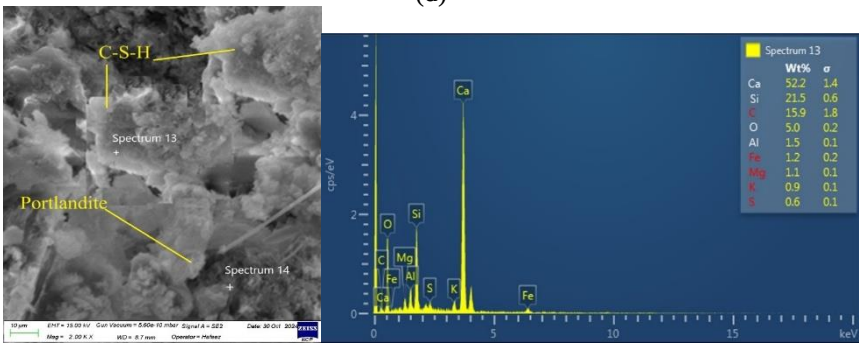

(e)

Fig. 6 SEM images and EDS of mixes (a) PC70SF30MK0MFA0 (b) PC70SF20MK10MFA0 (c) PC70SF0MK30MFA0 (d) PC70SF20MK0MFA10 (e) PC70SF0MK0MFA30

the formation of a microporous network interspersed with discrete crystals within the pores, attributed to the calcium-aluminum-silicate hydrate gel. EDS detected Fe-containing crystals up to 5 µm, likely associated with AFm phases originating from C4AF (tetracalcium aluminoferrite) (Taylor 1997).

For the PC70SF20MK10MFA0 mixture, the compressive strength of 129.2 MPa can be linked to the synergistic effect of SF and MK, which generated a calcium silicate hydrate gel with homogeneity similar to that of PC70SF30MK0MFA0. The formation of an acicular crystal network within the pores, enriched in Ca, Al, Si, and S, corresponds to the presence of hydrated SO4-AFm phases (OH^-). Additionally, small, irregularly spaced hexagonal scalenohedral crystals with rough and brittle surfaces were observed. These crystals likely formed during the later stages of secondary calcium silicate hydrate transformation due to portlandite precipitation and are rich in Ca, Si, and Al (Stoppa *et al*. 2010).

The high MK content in the PC70SF0MK30MFA0 mixture is responsible for the matrix's granular texture and disruptions in the formation of calcium silicate hydrate (C-S-H) and cement bonding. Consequently, after 28 days, this composition exhibited a lower compressive strength (CS) of 117 MPa compared to PC70SF30MK0MFA0 and PC70SF20MK10MFA0. Within the pores, radially arranged acicular crystals, identified as aragonite, were observed. Based on decarbonized mass analyses, XRD, and TGA measurements, these crystals appear to preferentially precipitate under heat-curing conditions. Stratlingite was characterized by thin, folded, flaky plates with hexagonal or pseudo-hexagonal geometries, and EDS analysis confirmed the presence of Ca, Si, and Al. The sulfur content detected is likely linked to the SO_4-AFm structure, stemming from partial ionic replacement of gypsum granules originating from the clinker (Okoronkwo and Glasser 2016a, Okoronkwo *et al*. 2021).

The inclusion of MFA in PC70SF20MK0MFA10 promoted a rigid matrix due to an optimal particle size distribution, producing a microstructure similar to that of PC70SF20MK10MFA0 (He *et al*. 2018). After 28 days, this led to a CS of 129.9 MPa, although increased heterogeneity was noted due to the filler acting as nucleation sites enveloped by C-S-H. XRD, TGA, and prior studies (Liu *et al*. 2020) indicate that adding MFA to PC70SF0MK0MFA30 generated a coarser microstructure, attributed to weak bonding between hydrates and MFA within the C-S-H gel, resulting in higher pore content, portlandite, and unhydrated phases. Within the pores of PC70SF20MK0MFA10, hydrates containing Si, Ca, and Al were observed, corresponding to stratlingite in various metastable forms, including needle-like aggregates and the subsequent development of pseudo-hexagonal leaflets. Compared with PC70SF0MK30MFA0, this structure displayed larger dimensions, influenced by the presence of MFA, which reduced solubility in the matrix.

As observed in PC70SF30MK0MFA0, incorporating SF significantly densified the matrix, enhancing strength and reducing porosity. XRD results indicated similar precipitation of residual anhydrous C3S phases and no major defects near the aggregate. Likewise, MK in PC70SF0MK30MFA0 exerted a comparable effect on the hydrated matrix as SF in PC70SF30MK0MFA0 (Abdellatief *et al*. 2023). Reduced strengths at 7 and 28 days in PC70SF0MK0MFA30 were linked to heightened microstructural heterogeneity caused by MFA addition, which is explained by the non-spherical particle morphology and the dilution of nucleation sites, leading to discontinuities within the matrix (Yusuf *et al*. 2022).

3.6 X-ray Diffraction (XRD)

X-ray diffraction (XRD) analysis was employed to examine hydrate formation in the UHPGC mixtures after 28 days of curing. The results are illustrated in Fig. 7. Gismondine was detected as the dominant argillomineral within the 25°–35° (2θ) range for the compositions PC70SF20MK10MFA0, PC70SF20MK0MFA10, and PC70SF0MK0MFA30, indicating phases associated with calcium-aluminum-silicate hydrate (C-A-S-H) gel (Wetzel and Middendorf 2019). All UHPGC formulations investigated in this study exhibited gismondine presence. Its formation was influenced by several factors, including the mass ratios of the component combinations and the application of heat curing at 60 °C.

The emergence of additional precipitates in PC70SF0MK30MFA0 and PC70SF30MK0MFA0 suggests that using a single SCMs can interfere with gismondine crystallization, likely due to modifications in the Ca/Si ratio. Since no portlandite (CH) peaks were observed, the mixes PC70SF20MK10MFA0, PC70SF20MK0MFA10, PC70SF0MK30MFA0, and PC70SF30MK0MFA0 demonstrated effective transformation of portlandite into this nanocrystalline phase. Furthermore, Okoronkwo reported that gismondine is found within calcium silicate hydrate phases with lower calcium content and in aluminosilicate gels after heat treatment between 20 and 85 °C, indicating that the curing regime used in the UHPGC systems was sufficient to facilitate gismondine formation.

Even in the PC70SF0MK0MFA30 mixture, where CH peaks were visible, gismondine formation still occurred. This is because gismondine dominates in this composition, as a combination of (Ca, Na) gismondine can react with alkalis and portlandite to produce calcium-aluminum-silicate hydrate and hydrogarnets (Yusuf, Al-Sodani *et al*. 2022). Comparable calcium silicate (CS) phases were reported by Kang *et al*. (2019), who also identified crystalline phases containing aluminates. These findings suggest that the precipitation of C-A-S-H compounds contributes to enhancing the compressive strength of the fortified matrix.

Consistent with prior studies on UHPGC systems (Liu *et al*. 2020, Qian *et al*. 2020), the diffractograms of all mixtures in this study indicated the presence of colloidal calcium silicate hydrate gel. Under ambient curing conditions, the crystalline peak of calcium silicate hydrate, originating from the hydration of alite (C3S) or belite (β-C2S), appeared near 50° (2θ) with a spacing of approximately 1.83 Å. Jennite displayed disordered characteristics, evidenced by broad, weak amorphous bands (Chen *et al*. 2004).

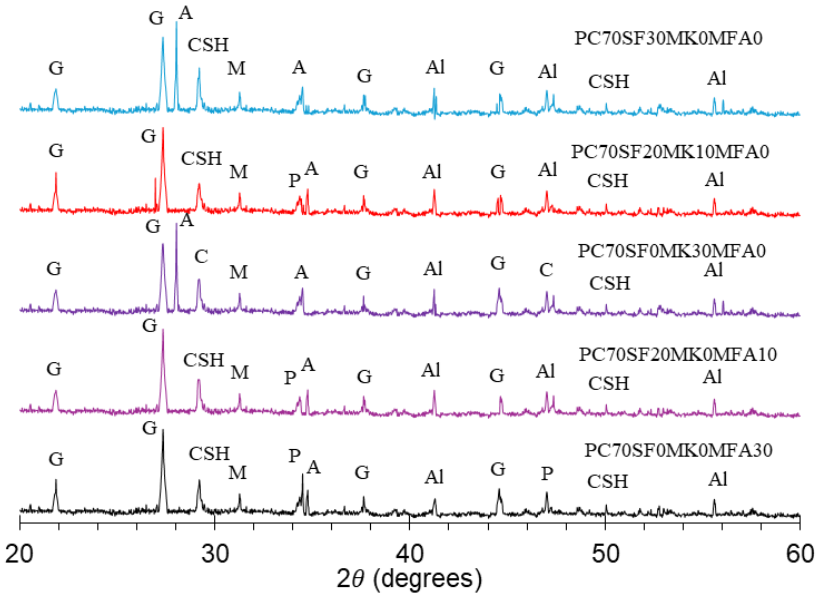

Fig. 7 XRD results of mixes (P: Portlandite, A: Anorthite, C: Calcite, M: Mullite, G: Gismondine, Al: Alite)

All compositions exhibited residual alite, representing unhydrated tricalcium silicate from Portland cement (Ren *et al*. 2013, Tafraoui *et al*. 2016), consistent with observations in multiple studies (Zhang *et al*. 2018, He *et al*. 2020, Mo *et al*. 2020, Sohail *et al*. 2021). According to Sohail *et al*. (2021), PC70SF0MK30MFA0 and PC70SF30MK0MFA0 showed strong XRD peaks, whereas PC70SF20MK10MFA0, PC70SF20MK0MFA10, and PC70SF0MK0MFA30 exhibited weaker, accessory peaks, reflecting the formation of distinct calcium silicate hydrate phases through pozzolanic reactions and cement hydration. This suggests that the low water-to-binder ratio in the UHPGC matrix contributed to a significant fraction of unhydrated clinker remaining after 28 days (Wang *et al*. 2019). In the PC70SF0MK0MFA30 composition, the reduced intensity of C3S peaks, compared to other mixtures, may be attributed to the enhanced solubility of clinker phases caused by the high alkali content of MFA (Vaitkevičius *et al*. 2014).

The mixture exhibiting the lowest mechanical strength, PC70SF0MK0MFA30, was unique in showing the highest content of Portlandite. The presence of this phase in UHPGC systems has been reported in multiple studies (Huang *et al*. 2017, Dixit *et al*. 2020, He *et al*. 2020, Qian *et al*. 2020). In UHPGC matrices that lack significant pozzolanic reactions, which typically consume CH, Portlandite often accumulates. Its presence tends to weaken the nanocrystalline network, making it less stable (Barzgar *et al*. 2021). Among the studied compositions, only PC70SF0MK30MFA0 displayed evidence of calcite formation, corroborating previous UHPGC findings (Huang *et al*. 2017, Zhang *et al*. 2018). This is attributed to the reaction of anhydride with CH, producing water and carbonate species (Santos *et al*. 2020). Moreover, when calcium silicate hydrate interacts with CO2 or $CO3^{2-}$ ions to form calcite, it disrupts the C-S-H structure, generates hydrated silica, and reduces the Ca/Si ratio, which explains the lower CS observed compared to PC70SF30MK0MFA0.

In PC70SF30MK0MFA0, the presence of amorphous silica suggests that gismondine forms through reactions with C3A and C4AF. This indicates that only part of the CH was converted into new phases, while a fraction of the mineral additives remained unreacted, as C3S mainly precipitated within the matrix (Yusuf *et al*. 2022). The distinct Ca/Si ratios observed in the diffraction data for the ternary systems PC70SF20MK10MFA0 and PC70SF20MK0MFA10 point to a predominance of gismondine. This highlights that the addition of MK and MFA can promote the development of hydrogarnet phases.

3.7 Thermogravimetric analysis with differential thermogravimetry (TGA/DTG)

The TGA/DTG analyses of the mixes at 7, 14, and 28 days are presented in Figure 8. Peaks observed in the DTG curves of all UHPGC matrices between 80 and 100 °C correspond to the loss of free water and the dehydration of AFm phases, including carboaluminate and monosulphate species. Monosulfoaluminate is identified as the predominant phase among these precipitates. Additionally, during this process, some hydrates within the calcium silicate hydrate (C-S-H) gel form when SO_4^{2-} ions are replaced by OH^- or CO_3^{2-} ions (de Matos et al. 2020, He et al. 2020). In the DTG curves for PC70SF20MK0MFA10, PC70SF0MK0MFA30, and PC70SF0MK30MFA0 across all curing ages, a further dehydration event is observed between 150 °C and 200 °C, attributable to the formation of stratlingite. This occurs when gismondine interacts with SO_4-AFm via structural ion substitution. These substitutions, primarily involving carbonate and sulfate anions, result in the formation of solid solutions and hydroxide variants (Okoronkwo and Glasser 2016b, Okoronkwo *et al*. 2021). This observation aligns with previous studies reporting the presence of amorphous C-A-S-H gel in the same dehydration range (Mo *et al*. 2020, Garcia-Lodeiro *et al*. 2021, Zhao *et al*. 2021).

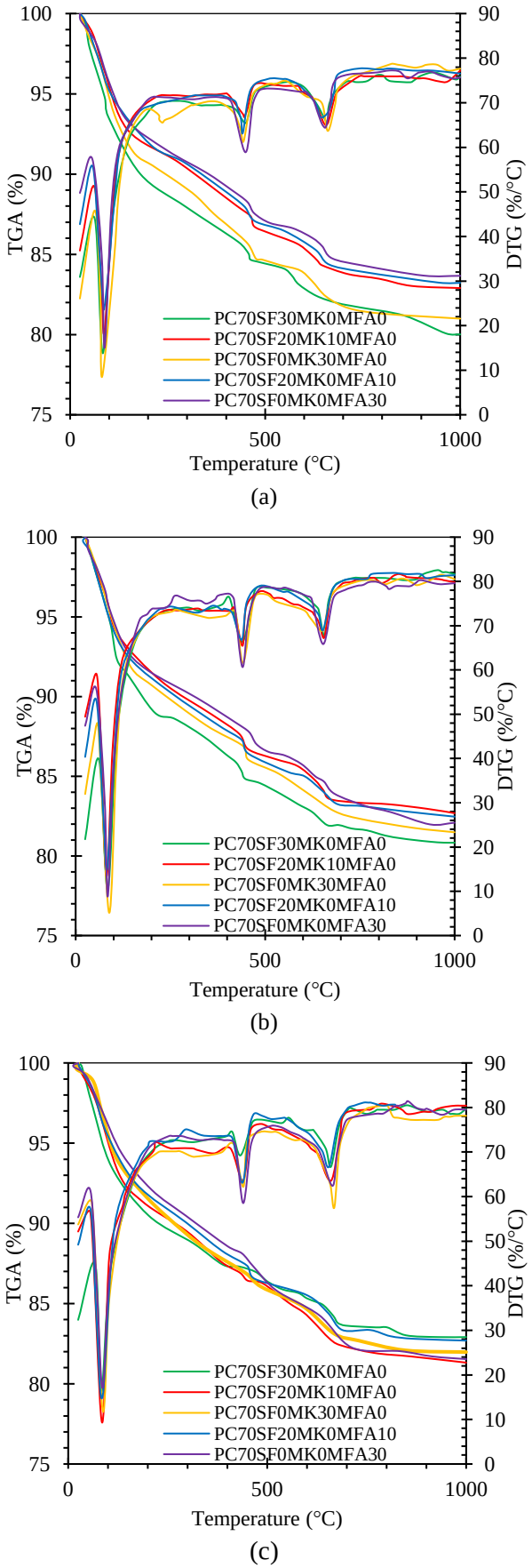

Fig. 8 TGA and DTG analysis at (a) 7 days, (b) 14 days, and (c) 28 days

It can be inferred that gismondine did not interact with monosulphates in the PC70SF20MK10MFA0 and PC70SF30MK0MFA0 mixes, as the DTG curves at 7, 14, and 28 days showed no dehydration peaks between 150 °C and 200 °C. Instead, within the calcium silicate hydrate (C-S-H) gel, hydroxyl or carbonate ions preferentially substituted for SO_4^{2-} ions. This behavior is attributed to the chemical incompatibility between gismondine and SO_4-AFm, which prevents their coexistence within the C-A-S-H matrix (Okoronkwo *et al*. 2021). DTG analysis across all mixtures revealed that various C-S-H gel-related phases with higher thermal stability underwent dehydration in the 250–400 °C range (He *et al*. 2020, Zhang *et al*. 2023). This is likely due to the formation of new crystalline phases in the matrix, potentially driven by decalcification of the C-S-H gel (Garcia-Lodeiro *et al*. 2021). Specifically, gismondine induced multiple dehydration events, predominantly between 310 °C and 390 °C, and its presence was confirmed by a distinct DTG peak at 335 °C for PC70SF20MK0MFA10 at 28 days.

For PC70SF0MK30MFA0 at 7 days, the DTG curve showed a thermal event at 245 °C corresponding to calcium aluminate hydrate (CAH), a phase typically formed in MK-containing cementitious systems. However, this feature was absent at 14 and 28 days, indicating that CAH formation is limited to early hydration stages, driven by sulfate interactions with C_3A.

Comparing the mixes, PC70SF30MK0MFA0, PC70SF0MK30MFA0, and PC70SF0MK0MFA30 exhibited simpler water release from C-S-H hydrates than PC70SF20MK10MFA0 and PC70SF20MK0MFA10. The dominance of C_3S in PC70SF0MK0MFA30 delayed clinker hydration and CH crystallization, generating less stable reactions, while XRD patterns for PC70SF0MK30MFA0 and PC70SF30MK0MFA0 indicated the highest mass losses. This observation is consistent with their higher degree of hydration (DH) relative to the other mixes (de Matos *et al*. 2020). At 28 days, all samples had CH contents comparable to reported UHPGC systems achieving compressive strengths above 100 MPa (de Matos *et al*. 2020, Dixit *et al*. 2020).

The DH values calculated at 7, 14, and 28 days showed rapid early hydration within the first week, with only minor increases at later ages. This reflects the stabilization of the hydrated matrix and the residual unreacted C_3S, which gradually reacts over time. Similar trends have been reported, where elevated curing temperatures accelerate early hydration but limit further reactions at later ages (Yu, Spiesz *et al*. 2015, Dixit, Du *et al*. 2020). Furthermore, due to the low water-to-binder ratios, DH typically remains below 35% in standard UHPGC systems (Du, Wang *et al*. 2023).

Compositions containing MFA (PC70SF20MK0MFA10 and PC70SF0MK0MFA30) exhibited higher DH at 28 days than PC70SF30MK0MFA0, likely because the fine filler particles act as nucleation sites, promoting C-S-H formation and overall hydration (Chu *et al*. 2022). This aligns with Dixit *et al*. (2019), who observed notable internal curing effects even at low water-to-binder ratios. The high SF content in PC70SF30MK0MFA0 enhanced CH conversion

efficiency compared to the ternary mixes PC70SF20MK10MFA0 and PC70SF20MK0MFA10 due to improved hydrate packing within C-S-H and C-A-S-H gels. While MFA in PC70SF0MK0MFA30 promoted a linear increase in DH, the inclusion of MK in PC70SF0MK30MFA0 led to greater decarbonated mass accumulation. Additionally, the lack of monosulfoaluminate formation in PC70SF30MK0MFA0, evidenced by DTG curves, confirms that its formation is restricted to mixes containing MK and MFA.

4. Critical discussion

The results of this work demonstrate the intricate relationship that exists between the type of SCMs, the thermal curing regime, and the microstructural evolution that results in UHPGC. The shape and reactivity of SCMs, as well as their cooperative interaction under heat-cured conditions, significantly influence the trends in mechanical and durability performance that have been observed. Superior compressive strength, less capillary water absorption, and low drying shrinkage were the outcomes of the densest and most refined matrix structure produced by the addition of SF. According to other studies (Richard and Cheyrezy 1995, Soliman and Tagnit-Hamou 2017), SF's ultrafine particle size and high amorphous silica concentration facilitate the development of C-A-S-H and C/N-A-S-H gels, which is why this result is consistent with previous research. The increased impermeability and early-age strength attained by SF integration further support the crucial function of reactive silica in lowering porosity and speeding up geopolymerization.

MK, on the other hand, demonstrated decreased workability and marginally worse strength performance in spite of its high alumina content and role in the creation of geopolymer gel. This is explained by MK's erratic particle shape and slower rate of breakdown, which would have prevented dense hydrated products from forming completely. The ability of MK to support long-term structural stability was validated by the increased microstructural compactness and secondary reaction phases shown by the binary and ternary blends containing MK. Khater (2016) and Moula *et al*. (2023) showed similar patterns, suggesting that MK-rich systems promote the slow polymerization of aluminosilicate gels that improve durability at later ages.

Despite being weaker than SF, MFA's performance highlights its potential as a long-term SCM in UHPGC. Its incorporation improved flowability by more than 35%, demonstrating that MFA's spherical shape and low water absorption boost mix rheology and particle packing. MFA-containing systems met ultra-high performance requirements by achieving compressive strengths of over 100 MPa, despite a moderate strength drop of roughly 23% when compared to SF-based mixtures. According to Lv *et al*. (2022) and Chu *et al*. (2024), inadequate reaction and decreased pozzolanic activity are the causes of the somewhat increased porosity and residual portlandite content seen in MFA-rich mixes. However, MFA demonstrated distinct synergistic benefits in ternary mixes with SF or MK, balancing microstructural densification, strength, and workability.

Early hydration and subsequent reactions were greatly aided by the 48-hour thermal curing at 60 °C, which produced the calcite and gismondine phases that thickened the binder matrix. The mild curing regime used in this investigation produced equivalent strength while using less energy than high-temperature curing (>90 °C) described in the literature (Zhang *et al*. 2019, Wu *et al*. 2017), indicating a feasible route for prefabricated UHPGC applications. Controlled heat treatment improves interfacial bonding and decreases microcrack development, especially in SF-rich and ternary systems, as shown by the densification effect seen by SEM/EDS and XRD.

Overall, this study shows that although SF is still the most common strength-enhancing SCM, cost, sustainability, and mechanical performance may all be successfully balanced by integrating MFA and MK in the right amounts. The ternary formulation (PC70SF20MK10MFA0 and PC70SF20MK0MFA10) achieves high strength (about 130 MPa), superior workability, and decreased permeability, making it the ideal compromise. When performance and environmental efficiency are crucial for large-scale precast or modular construction, this synergy provides a sustainable substitute for entirely SF-based UHPGC.

5. Conclusions

This research investigated the mechanical and microstructural behavior of thermally cured ultra-high-performance geopolymer composites (UHPGC) incorporating municipal solid waste incineration fly ash (MFA) as a supplementary cementitious material (SCM). The results demonstrate that energy usage and curing periods can be reduced without compromising performance, with the principal findings summarized as follows:

1. MFA significantly better fresh-state workability in comparison to metakaolin (MK) and silica fume (SF). Workability improvements of 20.35% and 36.11% over SF- and MK-based composites were demonstrated by a mixture comprising 30% MFA. The MFA blend's density of 2337 kg/m³ was still appropriate for use in UHPGC applications.

2. All formulations reached compressive strengths above 100 MPa at 28 days. The SF-containing mixture achieved the highest strength (134.5 MPa) due to its superior reactivity, whereas the MFA-rich mix attained a respectable 109.3 MPa, highlighting MFA's potential as an eco-friendly alternative. A ternary combination (20% SF, 10% MK, 70% Portland cement) demonstrated a balanced performance with only minor reductions in strength.

3. Capillary water absorption (CWA) decreased markedly with SF incorporation, which promoted the formation of dense C-(A)-S-H and (C, N)-A-S-H gels. Thermal curing further enhanced impermeability by densifying the microstructure through calcite generation and improving interfacial transition zones, reducing porosity and enhancing durability.

4. SF also mitigated drying shrinkage by fostering gel

formation and filling pores, thereby strengthening matrix bonding and lowering porosity. Composites with higher SF content exhibited the lowest shrinkage, underscoring SF's role in improving dimensional stability.

5. Mixtures with elevated SF levels (e.g., PC70SF30MK0MFA0 and PC70SF20MK10MFA0) formed denser calcium silicate hydrate gels, achieving compressive strengths of 134.5 MPa and 129.2 MPa, respectively. Conversely, higher proportions of MK or MFA increased microporosity, weakening the composite structure.

6. In ternary mixes, gismondine became the main hydrate, and portlandite was transformed into nanocrystalline phases by optimal heat curing, which strengthened the microstructural stability. While MFA-dominant mixtures contained residual portlandite, which accounted for their somewhat poorer performance, thermal studies showed less portlandite and effective secondary hydration in SF-rich composites.

7. Future investigations should focus on optimizing MFA pre-treatment techniques and curing protocols to boost reactivity and minimize porosity in UHPGC. Additionally, long-term durability under aggressive conditions, CO_2-curing strategies, and comprehensive life cycle assessments are necessary to establish MFA-based UHPGC as a sustainable, high-performance material suitable for large-scale construction projects.

Although this study shows that adding MFA to UHPGC during thermal curing results in dense microstructures and strengths greater than 100 MPa, it should be highlighted that there are a number of restrictions. Generalization was limited by the study's use of a single curing regime (60 °C for 48 hours) and 30% MFA substitution. Long-term exposure testing were not conducted, only short-term mechanical and durability performances were evaluated. The energy and water requirements of the MFA pre-treatment process may limit its large-scale use. Furthermore, only SEM/EDS, XRD, and TGA were used for microstructural investigation, which calls for additional pore structure and nano-mechanical characterisation in subsequent research.

Acknowledgment

The authors extend their appreciation to the Deanship of Research and Graduate Studies at King Khalid University for funding this work through a Large Research Project under grant number RGP 2/285/46. The authors extend their appreciation to the Deanship of Scientific Research at Northern Border University, Arar, KSA for funding this research work through the project number "NBU-FFMRA-2025-2105-15

References

Abdellatief, M., M. Abd Elrahman, G. Elgendy, G. Bassioni and A.M. Tahwia (2023), "Response surface methodology-based modelling and optimization of sustainable UHPC containing ultrafine fly ash and metakaolin", *Constr. Build. Mater.*, **388**, 131696. https://doi.org/10.1016/j.conbuildmat.2023.131696

Akbar, D., Shabir, F., Raza, A. and Kahla, N.B. (2025), "Synergistic enhancement of recycled aggregate concrete using hybrid natural-synthetic fiber reinforcement and silica fume", *Results Eng.*, **27**, 106291. https://doi.org/10.1016/j.rineng.2025.106291

Aydogdu, M. (2014), "On the vibration of aligned carbon nanotube reinforced composite beams", *Adv. Nano Res.*, **2**(4), 199. https://doi.org/10.12989/anr.2014.2.4.199

Abellan-Garcia, J., M.I. Khan, Y.M. Abbas, A. Castro-Cabeza and J. Carrillo (2023), "Multi-criterion optimization of low-cost, self-compacted and eco-friendly micro-calcium-carbonate-and waste-glass-flour-based Ultrahigh-Performance concrete", *Constr. Build. Mater.*, **371**, 130793. https://doi.org/10.1016/j.conbuildmat.2023.130793

Adnan, A., M.T. Farooq, Y.S. Pervez, A. Raza and M. Arshad (2024), "Structural efficiency of fiber-reinforced geopolymer concrete confined with CFRP sheets", *Tech. J.*, **3**(ICACEE), 158-165.

Ahmad, S., K.O. Mohaisen, S.K. Adekunle, S.U. Al-Dulaijan and M. Maslehuddin (2019), "Influence of admixing natural pozzolan as partial replacement of cement and microsilica in UHPC mixtures", *Constr. Build. Mater.*, **198**, 437-444. https://doi.org/10.1016/j.conbuildmat.2018.11.260

Ahmed, M., A. Selmi, N. Ghazouani, A. Raza and A. Mabrouk (2024), "Mechanical and microstructural characterization of molybdenum tailings-, GGBS-and recycled aggregate based-low carbon self-compacting concrete", *Mater. Lett.*, 137960. https://doi.org/10.1016/j.matlet.2024.137960

Al-Naghi, A.A.A., Y. Alashker, N. Ghazouani, A. Selmi and A. Raza (2025a), "Mechanical and microstructural characteristics of fly ash-based concrete having copper-zinc oxide and graphitic carbon nitride hybrid composites", *Mater. Lett.*, 137986. https://doi.org/10.1016/j.matlet.2025.137986

Al-Naghi, A.A.A., N. Ghazouani, A. Selmi, Y. Alashker and A. Raza (2025b), "Combined effects of elevated temperature, sulfates and chlorides on performance of fly ash and metakaolin-based recycled aggregate geopolymer concrete", *J. Build. Eng.*, **99**, 111561. https://doi.org/10.1016/j.jobe.2024.111561

Al-Naghi, A.A.A., N. Ghazouani, A. Selmi, A. Raza and M. Ahmed (2024), "Mechanical and microstructural characterization of recycled aggregate geopolymer concrete having high strength and recycled tire steel wire fibers", *Mater. Lett.*, 137787. https://doi.org/10.1016/j.matlet.2024.137787

Al-Tikrite, A. and M. N. Hadi (2017), "Mechanical properties of reactive powder concrete containing industrial and waste steel fibres at different ratios under compression", *Constr. Build. Mater.*, **154**, 1024-1034. https://doi.org/10.1016/j.conbuildmat.2017.08.024

Alashker, Y., A. Selmi, A. Raza and N. Ghazouani (2025), "Microstructural and thermal characterization of polyethylene and basalt fiber-reinforced natural zeolite-based engineered geopolymer composites", *Mater. Lett.*, 137984. https://doi.org/10.1016/j.matlet.2025.137984

ASTM, A. (2023), "Standard specification for flow table for use in tests of hydraulic cement", ASTM West Conshohocken **1**.

ASTM, A. (2024), "C138/C138M—23 Standard test method for density (unit weight), yield, and air content (gravimetric) of concrete", ASTM Int **6**.

ASTM, C. (2007), "Standard practice for making and curing concrete test specimens in the laboratory", C192/C192M.

Bakharev, T., J.G. Sanjayan and Y.B. Cheng (1999), "Alkali activation of Australian slag cements", *Cement Concr. Res.*, **29**(1), 113-120. https://doi.org/10.1016/S0008-8846(98)00170-7

Barzgar, S., M. Tarik, C. Ludwig and B. Lothenbach (2021), "The effect of equilibration time on Al uptake in CSH", *Cement*

Concr. *Res*., **144**, 106438. https://doi.org/10.1016/j.cemconres.2021.106438

Beltrame, N.A.M., R.L. Dias, F.B. Witzke and R.A. Medeiros-Junior (2023), "Effect of carbonation curing on the physical, mechanical, and microstructural properties of metakaolin-based geopolymer concrete", *Constr*. *Build*. *Mater*., **406**, 133403. https://doi.org/10.1016/j.conbuildmat.2023.133403

C39/C39M-18, A. (2018), *Standard Test Method for Compressive Strength of Cylindrical Concrete Specimens*, ASTM International, West Conshohocken, PA.

C-13, A. (2013), "Standard test method for measurement of rate of absorption of water by hydraulic-cement concretes", *ASTM Int* **41**(147), 1-6.

Castel, A., S. Foster, T. Ng, J. Sanjayan and R. Gilbert (2016), "Creep and drying shrinkage of a blended slag and low calcium fly ash geopolymer Concrete", *Mater*. *Struct*., **49**, 1619-1628. https://doi.org/10.1617/s11527-015-0599-1

Chen, J.J., J.J. Thomas, H.F. Taylor and H.M. Jennings (2004), "Solubility and structure of calcium silicate hydrate", *Cement Concr*. *Res*., **34**(9), 1499-1519. https://doi.org/10.1016/j.cemconres.2004.04.034

Chu, H., Y. Gu, W. Shi and J. Jiang (2024), "Assessing the performance and sustainability of ecological mortar with municipal solid waste incineration fly ash solidified by sulphoaluminate cement", *Constr*. *Build*. *Mater*., **450**, 138613. https://doi.org/10.1016/j.conbuildmat.2024.138613

Chu, S., L. Li, P. Shen, J. Lu and C. S. Poon (2022), "Recycling of waste glass powder as paste replacement in green UHPFRC", *Constr*. *Build*. *Mater*., **316**, 125719. https://doi.org/10.1016/j.conbuildmat.2021.125719

de Matos, P.R., R.D. Sakata, P.J.P. Gleize, J. de Brito and W.L. Repette (2020), "Eco-friendly ultra-high performance cement pastes produced with quarry wastes as alternative fillers", *J*. *Clean*. *Prod*., **269**, 122308. https://doi.org/10.1016/j.jclepro.2020.122308

Dixit, A., H. Du and S. Dai Pang (2020), "Marine clay in ultra-high performance concrete for filler substitution", *Constr*. *Build*. *Mater*., **263**, 120250. https://doi.org/10.1016/j.conbuildmat.2020.120250

Dixit, A., S. Gupta, S. Dai Pang and H. W. Kua (2019), "Waste Valorisation using biochar for cement replacement and internal curing in ultra-high performance concrete", *J*. *Clean*. *Prod*., **238**, 117876. https://doi.org/10.1016/j.jclepro.2019.117876

Dong, Y. (2018), "Performance assessment and design of ultra-high performance concrete (UHPC) structures incorporating life-cycle cost and environmental impacts", *Constr*. *Build*. *Mater*., **167**, 414-425. https://doi.org/10.1016/j.conbuildmat.2018.02.037

Du, J., Y. Wang, Y. Bao, D. Sarkar and W. Meng (2023), "Valorization of wasted-derived biochar in ultra-high-performance concrete (UHPC): pretreatment, characterization, and environmental benefits", *Constr*. *Build*. *Mater*., **409**, 133839. https://doi.org/10.1016/j.conbuildmat.2023.133839

Elhag, A.B., Ghazouani, N. and Raza, A. (2025), "Enhancing geopolymer properties with mineral wool waste: mechanical, microstructural, and thermal insights", *JOM*, 1-15. https://doi.org/10.1007/s11837-025-07726-z

Elhadi, K.M., A. Raza, N. Ghazouani, M. Yaqub and A. Mabrouk (2024), "Material characterization of high-ductility geopolymer composites developed with industrial and construction & demolition wastes", *Mater*. *Lett*., 137961. https://doi.org/10.1016/j.matlet.2024.137961

Fan, D., J. Zhu, M. Fan, J.X. Lu, S. Chu, E. Dong and R. Yu (2023), "Intelligent design and manufacturing of ultra-high performance concrete (UHPC)–A review", *Constr*. *Build*. *Mater*., **385**, 131495. https://doi.org/10.1016/j.conbuildmat.2023.131495

Farazin, A. and M. Mohammadimehr (2020), "Nano research for investigating the effect of SWCNTs dimensions on the properties of the simulated nanocomposites, a molecular dynamics simulation", *Adv*. *Nano Res*., **9**(2), 83-90. https://doi.org/10.12989/anr.2020.9.2.083

Garcia-Lodeiro, I., G. Goracci, J.S. Dolado and M.T. Blanco-Varela (2021), "Mineralogical and microstructural alterations in a portland cement paste after an accelerated decalcification process", *Cement Concr*. *Res*., **140**, 106312. https://doi.org/10.1016/j.cemconres.2020.106312

Ghazouani, N., A. Selmi, A. Raza, A.B. Elhag, F. Shabbir and F. Zahra (2024), "Mechanical strength and mineralogical properties of fiber-reinforced geopolymer composites with multi-walled carbon nanotubes", *Mater*. *Lett*., ***382***, 137843. https://doi.org/10.1016/j.matlet.2024.137843

Ghazouani, N., Ibrahim, W.M., Alsulamy, S. and Raza, A. (2025). Compressive toughening and microstructural assessment of glass fiber reinforced phosphate-activated kaolinitic geopolymers. *Mater*. *Lett*., **398**, 138903. https://doi.org/10.1016/j.matlet.2025.138903

Guo, K.Z., G.Z. Zhang, Y. Li, J. Yang and Q.J. Ding (2024), "The mechanism of curing regimes on the macroscopic properties and microstructure of ultra-high performance concrete with lightweight aggregates", *J*. *Build*. *Eng*., **82**, 108236. https://doi.org/10.1016/j.jobe.2023.108236

He, Y., X. Zhang, S. Liu, R. Hooton, T. Ji and Y. Kong (2020), "Impacts of sulphates on rheological property and hydration performance of cement paste in the function of polycarboxylate superplasticizer", *Constr*. *Build*. *Mater*., **256**, 119428. https://doi.org/10.1016/j.conbuildmat.2020.119428

He, Z.H., S.G. Du and D. Chen (2018), "Microstructure of ultra high performance concrete containing lithium slag", *J*. *Hazard*. *Mater*., **353**, 35-43. https://doi.org/10.1016/j.jhazmat.2018.03.063

Hiremath, P. N. and S. C. Yaragal (2017), "Influence of mixing method, speed and duration on the fresh and hardened properties of Reactive Powder Concrete", *Constr*. *Build*. *Mater*., **141**, 271-288. https://doi.org/10.1016/j.conbuildmat.2017.03.009

Huang, S.J., S. Kannaiyan and M. Subramani (2022), "Effect of nano-Nb2O5 on the microstructure and mechanical properties of AZ31 alloy matrix nanocomposites", *Adv*. *Nano Res*., **13**(4), 407-416. https://doi.org/10.12989/anr.2022.13.4.407

Huang, W., H. Kazemi-Kamyab, W. Sun and K. Scrivener (2017), "Effect of cement substitution by limestone on the hydration and microstructural development of ultra-high performance concrete (UHPC)", *Cement Concr*. *Compos*., **77**, 86-101. https://doi.org/10.1016/j.cemconcomp.2016.12.009

Huang, X., Y. Tian, J. Jiang, X. Lu, Z. He and K. Jia (2024), "Mechanical properties and enhancement mechanism of iron ore tailings as aggregate for manufacturing ultra-high performance geopolymer concrete", *Constr*. *Build*. *Mater*., **439**, 137362. https://doi.org/10.1016/j.conbuildmat.2024.137362

Kamble, V., G. Kodwani, R. Sridharkrishna and B. Ankamwar (2014), "Synthesis of anisotropic defective polyaniline/silver nanocomposites", *Adv*. *Nano Res*., **2**(2), 111. https://doi.org/10.12989/anr.2014.2.2.111

Kang, S.H., S.G. Hong and J. Moon (2019), "The use of rice husk ash as reactive filler in ultra-high performance concrete", *Cement Concr*. *Res*., **115**: 389-400. https://doi.org/10.1016/j.cemconres.2018.09.004

Karataş, M., A. Benli and A. Ergin (2017), "Influence of ground pumice powder on the mechanical properties and durability of self-compacting mortars", *Constr*. *Build*. *Mater*., **150**, 467-479. https://doi.org/10.1016/j.conbuildmat.2017.05.220

Kahla, N.B., Ghazouani, N. and Raza, A. (2025), "Influence of phase change material on material characterization and thermal

behavior of engineered geopolymer composite", *JOM*, 1-10. https://doi.org/10.1007/s11837-025-07655-x

Khater, H. (2016), "Nano-Silica effect on the physicomechanical properties of geopolymer composites", *Adv. Nano Res.*, **4**(3), 181-195. https://doi.org/10.12989/anr.2016.4.3.181

Khater, H. and H. Abd El Gawwad (2015), "Effect of firing temperatures on alkali activated Geopolymer mortar doped with MWCNT", *Adv. Nano Res.*, **3**(4), 225. https://doi.org/10.12989/anr.2015.3.4.225

Li, F., Q. Chen, Y. Lu, Y. Zou and S. Li (2023), "Mitigating drying shrinkage and enhancing mechanical strength of fly ash-based geopolymer paste with functionalized MWCNTs grafted with silane coupling agent", *Cement Concr. Compos.*, **143**, 105250. https://doi.org/10.1016/j.cemconcomp.2023.105250

Liu, T., H. Wei, D. Zou, A. Zhou and H. Jian (2020), "Utilization of waste cathode ray tube funnel glass for ultra-high performance concrete", *J. Clean. Prod.*, **249**, 119333. https://doi.org/10.1016/j.jclepro.2019.119333

Lu, J.X., H.A. Ali, Y. Jiang, X. Guan, P. Shen, P. Chen and C.S. Poon (2022), "A novel high-performance lightweight concrete prepared with glass-UHPC and lightweight microspheres, Towards energy conservation in buildings", *Compos. Part B Eng.*, **247**, 110295. https://doi.org/10.1016/j.compositesb.2022.110295

Lv, Y., L. Yang, J. Wang, B. Zhan, Z. Xi, Y. Qin and D. Liao (2022), "Performance of ultra-high-performance concrete incorporating municipal solid waste incineration fly ash", *Case Stud. Constr. Mater.*, **17**, e01155. https://doi.org/10.1016/j.cscm.2022.e01155

Mabrouk, A., A. Raza, K. M. Elhadi, B. Ahmed, J. Kubica and W. Chen (2024), "Effect of curing temperature, silica fume, and waste tire rubber aggregate on material characterization of lightweight geopolymer composite", *Constr. Build. Mater.*, **453**, 139063. https://doi.org/10.1016/j.conbuildmat.2024.139063

Mo, Z., R. Wang and X. Gao (2020), "Hydration and mechanical properties of UHPC matrix containing limestone and different levels of metakaolin", *Constr. Build. Mater.*, **256**, 119454. https://doi.org/10.1016/j.conbuildmat.2020.119454

Moula, S., A.B. Fraj, T. Wattez, M. Bouasker and N.B.H. Ali (2023), "Mechanical properties, carbon footprint and cost of ultra-high performance concrete containing ground granulated blast furnace slag", *J. Build. Eng.*, **79**, 107796. https://doi.org/10.1016/j.jobe.2023.107796

Okoronkwo, M.U. and F.P. Glasser (2016a), "Stability of strätlingite in the CASH system", *Mater. Struct.*, **49**, 4305-4318. https://doi.org/10.1617/s11527-015-0789-x

Okoronkwo, M.U. and F.P. Glasser (2016b), "Strätlingite, compatibility with sulfate and carbonate cement phases", *Mater. Struct.*, **49**, 3569-3577. https://doi.org/10.1617/s11527-015-0740-1

Okoronkwo, M.U., S.K. Mondal, B. Wang, H. Ma and A. Kumar (2021), "Formation and stability of gismondine-type zeolite in cementitious systems", *J. Am. Ceram. Soc.*, **104**(3), 1513-1525.

Pyo, S., M. Tafesse, B.J. Kim and H.K. Kim (2018), "Effects of quartz-based mine tailings on characteristics and leaching behavior of ultra-high performance concrete", *Constr. Build. Mater.*, **166**, 110-117. https://doi.org/10.1016/j.conbuildmat.2018.01.087

Qian, D., R. Yu, Z. Shui, Y. Sun, C. Jiang, F. Zhou, M. Ding, X. Tong and Y. He (2020), "A novel development of green ultra-high performance concrete (UHPC) based on appropriate application of recycled cementitious material", *J. Clean. Prod.*, **261**, 121231. https://doi.org/10.1016/j.jclepro.2020.121231

Qu, Z., Q. Yu, Y. Ji, F. Gauvin and I. K. Voets (2020), "Mitigating shrinkage of alkali activated slag with biofilm", *Cement Concr. Res.*, **138**, 106234. https://doi.org/10.1016/j.cemconres.2020.106234

Raza, A., B. Ahmed, M.H. El Ouni and W. Chen (2024a), "Mechanical, durability and microstructural characterization of cost-effective polyethylene fiber-reinforced geopolymer concrete", *Constr. Build. Mater.*, **432**, 136661. https://doi.org/10.1016/j.conbuildmat.2024.136661

Raza, A., B. Ahmed, M.H. El Ouni, N. Ghazouani and W. Chen (2024b), "Microstructural and thermal characterization of polyethylene fiber-reinforced geopolymer composites", *J. Build. Eng.*, 109904. https://doi.org/10.1016/j.jobe.2024.109904

Raza, A., A. Salmi, M.H. El Ouni, N. Ghazouani, B. Ahmed and W. Chen (2024c), "Material characterization and thermal performance of polyethylene fiber-reinforced lightweight engineered geopolymer composites subjected to sulfate attacks", *Constr. Build. Mater.*, **455**, 139156. https://doi.org/10.1016/j.conbuildmat.2024.139156

Raza, A., Selmi, A., El Ouni, M. H. and Ghazouani, N. (2025a). Enhancing structural performance of hybrid fiber-reinforced geopolymer composites with AFRP confinement: Experimental, theoretical, and finite element analysis. *Constr. Build. Mater.*, **492**, 143063. https://doi.org/10.1016/j.conbuildmat.2025.143063

Raza, A., Ghazouani, N. and Ahmed, M. (2025b), "Lightweight engineered geopolymer composites with carbon nanotubes and lightweight aggregates: enhancing thermal resistance and mechanical strength", *JOM*, 1-12. https://doi.org/10.1007/s11837-025-07809-x

Raza, A., Ghazouani, N. and El Ouni, M. H. (2025c), "Enhancing thermal and mechanical resilience of self-compacting lightweight concrete with silica fume and hybrid basalt fibres", *Constr. Build. Mater.*, **494**, 143485. https://doi.org/10.1016/j.conbuildmat.2025.143485

Ren, F., C.H. Mattus, J.J.A. Wang and B.P. DiPaolo (2013), "Effect of projectile impact and penetration on the phase composition and microstructure of high performance concretes", *Cement Concr. Compos.*, **41**, 1-8. https://doi.org/10.1016/j.cemconcomp.2013.04.007

Richard, P. and M. Cheyrezy (1995), "Composition of reactive powder concretes", *Cement Concr. Res.*, **25**(7), 1501-1511. https://doi.org/10.1016/0008-8846(95)00144-2

Rößler, C., D.D. Bui and H.M. Ludwig (2014), "Rice husk ash as both pozzolanic admixture and internal curing agent in ultra-high performance concrete", *Cement Concr. Compos.*, **53**, 270-278. https://doi.org/10.1016/j.cemconcomp.2014.07.015

Salahaddin, S.D., J.H. Haido and G. Wardeh (2022), "The behavior of UHPC containing recycled glass waste in place of cementitious materials, A comprehensive review", *Case Stud. Constr. Mater.*, **7**, e01494. https://doi.org/10.1016/j.cscm.2022.e01494

Santos, B., D. Albuquerque and D. Ribeiro (2020), "Effect of the addition of metakaolin on the carbonation of Portland cement concretes", *Revista IBRACON de Estruturas e Materiais* **13**, 1-18.

Sohail, M.G., R. Kahraman, N. Al Nuaimi, B. Gencturk and W. Alnahhal (2021), "Durability characteristics of high and ultra-high performance concretes", *J. Build. Eng.*, **33**, 101669. https://doi.org/10.1016/j.jobe.2020.101669

Sokhandani, N., A.R. Setoodeh, S.M. Zebarjad, K. Nikbin and G. Wheatley (2022), "The influence of nano-silica on the wear and mechanical performance of vinyl-ester/glass fiber nano-composites", *Adv. Nano Res.*, **13**, 97-111. https://doi.org/10.12989/anr.2022.13.1.097

Soliman, N.A. and A. Tagnit-Hamou (2017), "Partial substitution of silica fume with fine glass powder in UHPC, Filling the micro gap", *Constr. Build. Mater.*, **139**, 374-383. https://doi.org/10.1016/j.conbuildmat.2017.02.084

Stoppa, F., F. Scordari, E. Mesto, V. Sharygin and G. Bortolozzi (2010), "Calcium-aluminum-silicate-hydrate "cement" phases

and rare Ca-zeolite association at Colle Fabbri, Central Italy", Open Geosciences **2**(2), 175-187.

Tafraoui, A., G. Escadeillas and T. Vidal (2016), "Durability of the ultra high performances concrete containing metakaolin", *Constr. Build. Mater.*, **112**, 980-987. https://doi.org/10.1016/j.conbuildmat.2016.02.169

Taylor, H. (1997). Cement chemistry, Thomas Telford.

Tran, T. M., H. T. Trinh, D. Nguyen, Q. Tao, S. Mali and T. M. Pham (2023), "Development of sustainable ultra-high-performance concrete containing ground granulated blast furnace slag and glass powder, Mix design investigation", *Constr. Build. Mater.*, **397**, 132358. https://doi.org/10.1016/j.conbuildmat.2023.132358

Vaitkevičius, V., E. Šerelis and H. Hilbig (2014), "The effect of glass powder on the microstructure of ultra high performance concrete", *Constr. Build. Mater.*, **68**, 102-109. https://doi.org/10.1016/j.conbuildmat.2014.05.101

Wang, X., R. Yu, Z. Shui, Q. Song, Z. Liu, Z. Liu and S. Wu (2019), "Optimized treatment of recycled construction and demolition waste in developing sustainable ultra-high performance concrete", *J. Clean. Prod.*, **221**, 805-816. https://doi.org/10.1016/j.jclepro.2019.02.201

Wetzel, A. and B. Middendorf (2019), "Influence of silica fume on properties of fresh and hardened ultra-high performance concrete based on alkali-activated slag", *Cement Concr. Compos.*, **100**, 53-59. https://doi.org/10.1016/j.cemconcomp.2019.03.023

Wu, H., M. He, S. Wu, J. Cheng, T. Wang, Y. Che, Y. Du and Q. Deng (2024), "Effects of binder component and curing regime on compressive strength, capillary water absorption, shrinkage and pore structure of geopolymer mortars", *Constr. Build. Mater.*, **442**, 137707. https://doi.org/10.1016/j.conbuildmat.2024.137707

Wu, Z., C. Shi and W. He (2017), "Comparative study on flexural properties of ultra-high performance concrete with supplementary cementitious materials under different curing regimes", *Constr. Build. Mater.*, **136**, 307-313. https://doi.org/10.1016/j.conbuildmat.2017.01.052

Yu, R., P. Spiesz and H. Brouwers (2015), "Development of an eco-friendly Ultra-High Performance Concrete (UHPC) with efficient cement and mineral admixtures uses", *Cement Concr. Compos.*, **55**, 383-394. https://doi.org/10.1016/j.cemconcomp.2014.09.024

Yusuf, M.O., K.A.A. Al-Sodani, A.A. Adewumi, A.H. Alateah, M.M. Al-Tholaia, S.M.I. Shamsah, U.Y. Qazi and G.D.S. Alanazi (2022), "Microstructural characteristics, modeling of mechanical strength and thermal performance of industrial waste glass blended concrete", *Appl. Sci.*, **12**(17), 8600.

Yusuf, M.O., K.A.A. Al-Sodani, A.H. AlAteah, M.M. Al-Tholaia, A.A. Adewumi, A.O. Bakare, A.K. Usman and I. Momohjimoh (2022), "Performances of the synergy of silica fume and waste glass powder in ternary blended concrete", *Appl. Sci.*, **12**(13), 6637. https://doi.org/10.3390/app12136637

Zhan, X., L. Tang, Z. Yue, H. Lu and J. Wang (2024), "Enhanced mechanical properties and mechanism of iron ore tailings-based geopolymers modified by municipal solid waste incineration fly ash", *J. Build. Eng.*, **98**, 111456. https://doi.org/10.1016/j.jobe.2024.111456

Zhang, C., S. Liu, P. Tang, X. Guan and C. Shi (2023), "Enhancing the hardening properties and microstructure of magnesium slag blocks by carbonation-hydration sequential curing", *J. Build. Eng.*, **76**, 107414. https://doi.org/10.1016/j.jobe.2023.107414

Zhang, D., A. Dasari and K. H. Tan (2018), "On the mechanism of prevention of explosive spalling in ultra-high performance concrete with polymer fibers", *Cement Concr. Res.*, **113**, 169-177. https://doi.org/10.1016/j.cemconres.2018.08.012

Zhang, G., G.F. Peng, X.Y. Zuo, X.J. Niu and H. Ding (2023), "Adding hydrated lime for improving microstructure and mechanical properties of mortar for ultra-high performance concrete", *Cement Concr. Res.*, **167**, 107130. https://doi.org/10.1016/j.cemconres.2023.107130

Zhang, H., T. Ji, B. He and L. He (2019), "Performance of ultra-high performance concrete (UHPC) with cement partially replaced by ground granite powder (GGP) under different curing conditions", *Constr. Build. Mater.*, **213**, 469-482. https://doi.org/10.1016/j.conbuildmat.2019.04.058

Zhang, Y., H. Liu, T. Ma, G. Gu, C. Chen and J. Hu (2023), "Understanding the changes in engineering behaviors and microstructure of FA-GBFS based geopolymer paste with addition of silica fume", *J. Build. Eng.*, **70**, 106450. https://doi.org/10.1016/j.jobe.2023.106450

Zhao, Y., J. Gao, Z. Xu, S. Li, X. Luo and G. Chen (2021), "Long-term hydration and microstructure evolution of blended cement containing ground granulated blast furnace slag and waste clay brick", *Cement Concr. Compos.*, **118**, 103982. https://doi.org/10.1016/j.cemconcomp.2021.103982

Zhou, T. and J. Li (2024), "Effect of lime neutralization wastewater on the performance of alkali-activated slag/fly ash mortars", *Mater. Struct.*, **57**(9), 1-11. https://doi.org/10.1617/s11527-024-02494-9

Zhu, Z., W. Huo, H. Sun, B. Ma and L. Yang (2023), "Correlations between unconfined compressive strength, sorptivity and pore structures for geopolymer based on SEM and MIP measurements", *J. Build. Eng.*, **67**, 106011. https://doi.org/10.1016/j.jobe.2023.106011

CC